JOC The Journal of Organic Chemistry

Featured Article

Cite This: J. Org. Chem. 2019, 84, 13221−13231

pubs.acs.org/joc

Disulfonimides versus Phosphoric Acids in Brønsted Acid Catalysis: The Effect of Weak Hydrogen Bonds and Multiple Acceptors on Complex Structures and Reactivity

Kerstin Rothermel,[§] Matej Žabka,[§] Johnny Hioe, and Ruth M. Gschwind*

Institute of Organic Chemistry, University of Regensburg, D-93053 Regensburg, Germany

Supporting Information

ABSTRACT: In Brønsted acid catalysis, hydrogen bonds play a crucial role for reactivity and selectivity. However, the contribution of weak hydrogen bonds or multiple acceptors has been unclear so far since it is extremely difficult to collect experimental evidence for weak hydrogen bonds. Here, our hydrogen bond and structural access to Brønsted acid/imine complexes was used to analyze BINOL-derived chiral disulfonimide (DSI)/imine complexes. ^{1}H and ^{15}N chemical shifts as well as $^{1}J_{NH}$ coupling constants revealed for DSI/imine complexes ion pairs with very weak hydrogen bonds. The high acidity of the DSIs leads to a significant weakening of the hydrogen bond as structural anchor. In addition, the five hydrogen bond acceptors of DSI allow an enormous mobility of the imine in the binary DSI complexes. Theoretical calculations predict the hydrogen bonds to oxygen to be energetically less favored; however, their considerable population is corroborated experimentally by NOE and exchange data. Furthermore, an *N*-alkylimine, which shows excellent reactivity and selectivity in reactions with DSI, reveals an enlarged structural space in complexes with the chiral phosphoric acid TRIP as potential explanation of its reduced reactivity and selectivity. Thus, considering factors such as flexibility and possible hydrogen bond sites is essential for catalyst development in Brønsted acid catalysis.

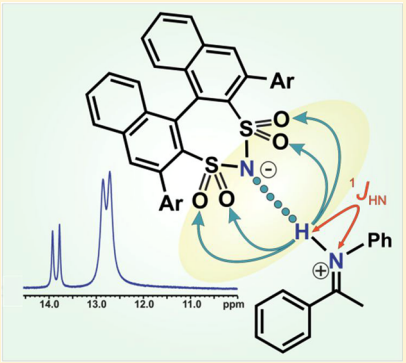

INTRODUCTION

In asymmetric synthesis, substrate activation by a chiral catalyst has been established as a powerful strategy.[1] In particular, BINOL-derived Brønsted acids constitute a class of robust, highly enantioselective, and extremely active catalysts available for many asymmetric transformations, including transfer hydrogenations, Strecker reactions, carbonyl additions, and many others.[1,2] One prominent example of these organocatalysts is chiral phosphoric acids (CPAs).[1] Extensive NMR studies of the binary complexes between different CPAs and aromatic *N*-arylimines proved the formation of strong, charge-assisted hydrogen bonds in these catalyst/substrate complexes, supported by a network of CH−π and π−π interactions.[3−5] Thus, the induced stereoselectivity stems from the noncovalent interactions.[6,7] However, for some transformations, even stronger Brønsted acids are required or at least show higher activities.[8−12]

For this purpose, the groups of List and others reported the synthesis[13−15] of disulfonimide catalysts (DSIs),[16] which are more acidic than the CPAs and were successfully applied as catalysts for the transfer hydrogenation of *N*-alkylimines.[9] Compared to *N*-arylamines, the formed products are more basic and slow the reaction by inhibiting the catalyst. In addition to the poor conversion, for the combination of CPA catalysts and *N*-alkylimines disappointing stereoselectivities were also observed. In contrast, the more acidic DSI catalysts provided both high turnovers and astonishingly good enantioselectivities.[9] In general, DSIs and other highly acidic catalysts have been applied in various reactions, in which the substrates are difficult to activate and the acidity of the CPAs is not sufficient.[17−19]

The assumed catalytic cycle for the transfer hydrogenation with *N*-alkylimines and DSI catalysts is similar to the proposed mechanism of the CPA catalyst transfer hydrogenation[21] and is shown in Figure 1. In the first step, the Brønsted acid catalyst **1** protonates the imine **2**, and a precatalytic species, the binary complex, is formed. Subsequently, the Hantzsch ester **3** reduces the imine, and the chiral amine **4** is formed as product. Finally, the catalyst **1** is regenerated by proton transfer.

In a Brønsted acid catalyzed Nazarov cyclization, a direct correlation between the pK_a values of the catalysts and the observed reaction rate was found.[22] For the cyclization, a faster reaction was observed for more acidic catalysts.[22] In one of our previous studies, the internal acidity of different CPAs was compared with the reactivity in the transfer hydrogenation of *N*-arylimines.[5] There, it was shown that the reaction with the least acidic CPA was the fastest, while the slowest reaction was observed with the most acidic CPA.[5] However, the most sterically hindered catalyst showed a drastic drop in reactivity. Since the formation of the binary complex (i.e., the binding of

Received: July 5, 2019
Published: September 24, 2019

DOI: 10.1021/acs.joc.9b01811
J. Org. Chem. 2019, 84, 13221−13231

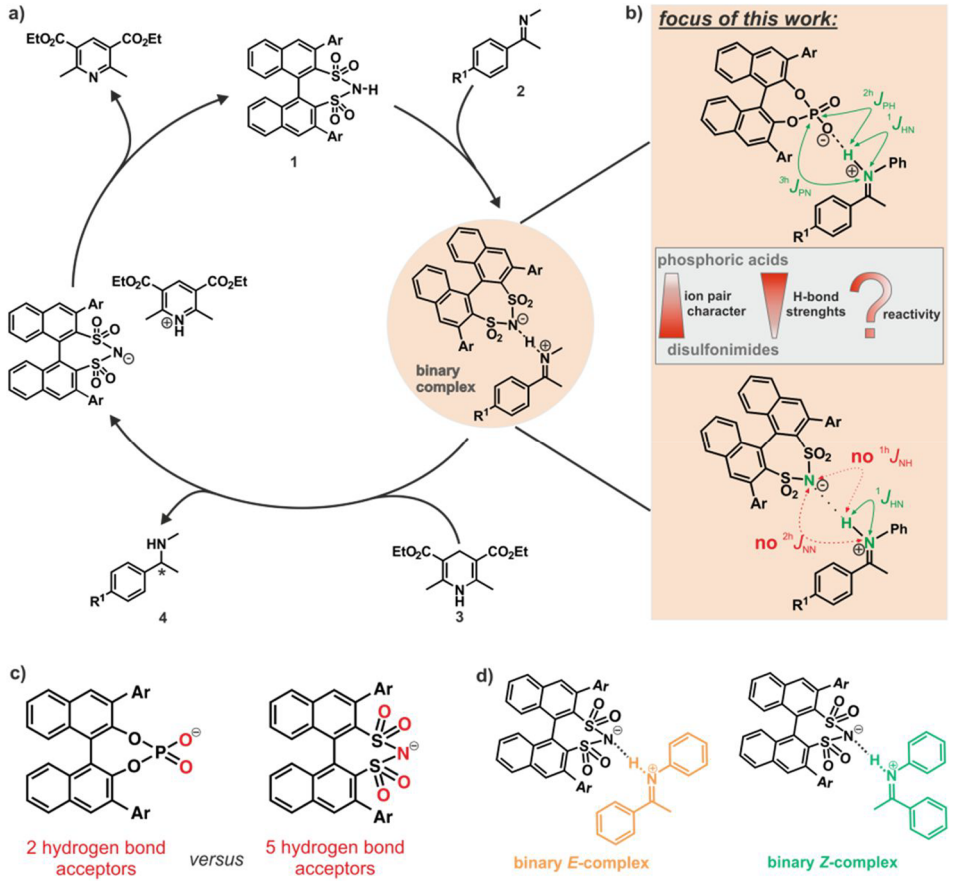

Figure 1. (a) Assumed catalytic cycle for the DSI-catalyzed asymmetric transfer hydrogenation of *N*-alkylimines **2** derived from that of CPAs. (b) The focus of this study was a hydrogen bond as well as a structural analysis of DSI/imine complexes regarding the influence of the weakened hydrogen bonds and the increased ion pair character. All results were compared to the previously investigated less acidic CPAs.[3−5,20] Finally, the internal acidity of these different classes of catalysts was correlated to the reactivity in the transfer hydrogenation. (c) In contrast to the CPAs, not only two but five possible hydrogen bond acceptors exist for the DSIs. (d) Investigated binary *E*-and *Z*-complexes are shown.

the imine) was similar to the other catalysts, most probably the binding of the Hantzsch ester is hindered.[5] This suggested that the reaction rate of the transfer hydrogenation is not only dependent on the internal acidity of the catalyst but can be also modulated by other factors such as the steric demand of the 3,3′-substituents and the corresponding size of the binding pocket.[5]

However, the use of stronger Brønsted acids raises the question of whether binary complexes with charge-assisted hydrogen bonds are present similar to the CPA/imine complexes[3,5] or whether pure ion pairs without hydrogen bond contribution are formed. As shown previously, the potential hydrogen bond is such a sensitive experimental indicator that the hydrogen bond analysis can give information about the binding situation and even small structural changes within the binary complexes can be derived.[3,5]

For CPA/imine complexes, four highly conserved core structures were observed experimentally. Thus, in solution, two different orientations (type I and type II) of each imine isomer (*E* and *Z*) inside the binary complex were detected.[4] The structural investigations of various CPA complexes showed that the 3,3′-substituents affect the relative population of these core structures but not their existence.[20] Despite the fact that low-temperature NMR spectroscopy was proven to be an excellent tool to investigate the occurring intermediates in Brønsted acid catalysis as well as the interactions between catalyst and substrates, until now, most of the NMR investigations have been confined to CPAs or their derivatives.[3−5,20,23,24] Similarly, the extensive computational studies within Brønsted acid catalysis focused mainly on CPAs.[7,25−32] However, to our knowledge, other acidic motifs and especially the promising DSI catalysts have not been examined.

Therefore, in this study, we investigated the binary complexes of two DSIs with two *N*-arylimines by low-temperature NMR spectroscopy. A detailed hydrogen bond analysis, regarding ^{1}H and ^{15}N chemical shifts and coupling constants, as well as structural investigations were conducted. These results are compared with the corresponding CPA/imine complexes. In particular, the effect of the increased number of hydrogen bond acceptors of the DSI compared to the CPA is addressed (Figure 1c). In addition, the differences of the more basic *N*-alkylimine in binary complexes with TRIP and DSI were compared. Finally, the expanded acidity range is correlated to the observed reaction rate in the transfer hydrogenation of imines.

RESULTS AND DISCUSSION

Model System. In order to compare the NHN hydrogen bonds of binary DSI/imine complexes with our previously investigated POHN hydrogen bonds of CPA/imine complexes,[3,4,20] a detailed hydrogen bond and structural analysis

DOI: 10.1021/acs.joc.9b01811
J. Org. Chem. 2019, 84, 13221−13231

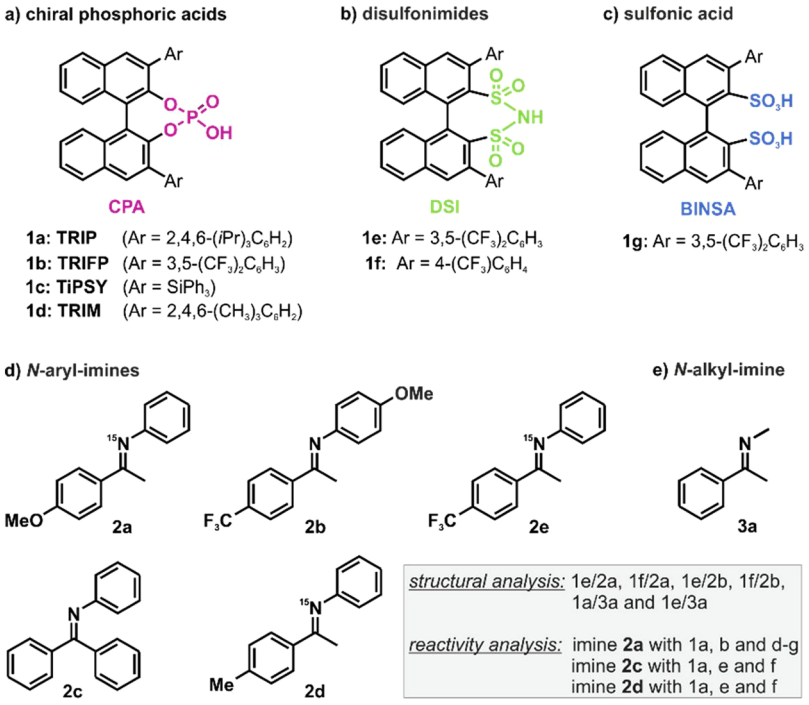

Figure 2. Binary complexes of different BINOL-derived Brønsted acids were analyzed. (a) While the phosphoric acids (CPAs) **1a**−**1d** were the main focus of our previous works,[3−5,20] (b) in this study the binary complexes between with the disulfonimides catalysts (DSIs) **1e** and **1f** were investigated. (c) In addition, the sulfonic acid (BINSA) **1g** was used for the reactivity analysis. (d) Hydrogen bond and structural analysis was done with imine **2a** and **2b**, whereas the reaction kinetics of imines **2a**, **2c**, and **2d** were investigated. (e) Additionally, also the hydrogen bonds between the *N*-alkylimine **3a** and CPA **1a** as well as DSI **1e** were investigated.

was conducted. As catalysts we selected the commercially available DSIs **1e** and **1f** (Figure 2). To enable a comparison with our previous structural investigations on CPA/imine complexes[3−5,20] and to reduce the severe chemical shift overlap the methoxy-substituted *N*-arylimines **2a** and **2b** were chosen. ^{15}N labeling of the imine **2a** allowed to access $^{1}J_{HN}$ coupling constants. Furthermore, the imines **2a**, **2c**, and **2d** were chosen for reactivity studies to consider the influence of electronic effects as well as isomerization. In addition, the highly acidic sulfonic acid (BINSA) **1g** was used in the reactivity comparison to expand the pK_a range of the catalysts even more. Finally, the more basic *N*-alkylimine **3a** was included in the structural investigations to address the special effects of *N*-alkyl versus *N*-arylimines known from synthetic applications.[9] To achieve the smallest possible signal line widths, all NMR measurements were conducted in CD_2Cl_2. All NMR spectra were recorded at 180 K to minimize exchange processes of the hydrogen-bonded protons.

Hydrogen Bond Analysis of the *N*-Aryl Imine Complexes. In general, the position of the proton within a hydrogen bond is dependent on the acidity of the hydrogen bond donor and the basicity of the acceptor. Thus, with increasing acidity of the donor the proton is initially shifted toward the center of the hydrogen bond, where the strongest hydrogen bonds are formed, then further on to the hydrogen bond acceptor resulting in a hydrogen bond assisted ion pair, and finally completely to the acceptor-forming pure ion pairs (Figure 3a). To define the position of the proton within OHN hydrogen bonds in pyridine/acid complexes, Steiner and Denisov developed an empirical correlation of ^{1}H and the ^{15}N chemical shifts.[33,34] Recently, we showed that this correlation is also applicable to the POHN hydrogen bonds in CPA/imine complexes.[3,5] For most of the binary CPA/imine complexes,

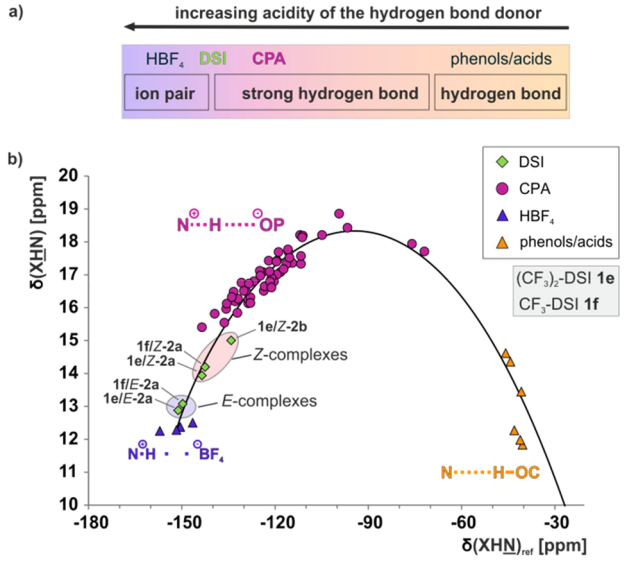

Figure 3. (a) With increasing acidity of the hydrogen bond donor, the proton is shifted toward the nitrogen of the hydrogen bond acceptor until an ion pair is formed. (b) Plot of $\delta_{(OHN)}$ against $\delta_{(OHN)}$ of the hydrogen-bonded complexes. The binary complexes of DSIs **1e** and **1f** with the imines **2a** and **2b** (green diamonds) are complemented with the binary imine complexes of HBF_4 (purple triangles), CPAs (pink cycles), and some carboxylic acids and phenols (orange triangles) from previous studies.[3,5] All ^{15}N chemical shifts are referenced [$\delta(OHN)_{ref} = \delta(OHN)_{exp} - 340$ ppm] (for details and exact values see the SI).

the ^{1}H chemical shifts of the hydrogen-bonded protons are above 16 ppm and follow a parabolic curve revealing very strong hydrogen bonds (Figure 3b).[3,5] The position on the left

DOI: 10.1021/acs.joc.9b01811
J. Org. Chem. 2019, 84, 13221−13231

upper half of the parabolic curve indicates hydrogen bond assisted ion pairs. In contrast to these CPA complexes, those with DSIs exhibit high field shifts for both ^{1}H and ^{15}N. As a result, the DSI/imine complexes are positioned far down on the left side of the Steiner−Limbach curve close to the almost pure ion pair with HBF_4 (Figure 3b). This position of the DSI complexes on the curve shows that the proton within the hydrogen bond is significantly shifted toward the nitrogen as expected for the more acidic DSI catalysts (Figure 3a). In general, ^{1}H and ^{15}N chemical shifts as well as the $^{1}J_{NH}$ coupling constants can be used to determine the hydrogen bond strengths. However, the ^{1}H chemical shift of the CPA/imine complexes was significantly influenced by neighborhood and shielding effects, whereas the ^{15}N chemical shift, which was directly correlated with the $^{1}J_{HN}$ coupling constant, is not so sensitive for these effects and could be used as an appropriate descriptor for the hydrogen bond strengths.[3,5] For this reason, the hydrogen-bond analysis of the DSI complexes was based on the ^{15}N chemical shifts. In particular, the *E*-configured DSI/**2a** complexes show a ^{15}N chemical shift, which is similar to the HBF_4 model system for purely ionic complexes, suggesting none or an extremely weak hydrogen bond. In contrast, for the investigated *Z* complexes with DSI a position on the curve significantly closer to the CPA catalysts was found, indicating a substantial contribution of a hydrogen bond within in these ion pairs (Figure 3b). Thus, the smaller sterical demand of the *Z*-imine leads to stronger hydrogen bonds in DSI complexes compared to the corresponding *E*-complexes. This observation is in accordance with the previously investigated CPA complexes, where calculated as well as experimentally derived atomic distances corroborated the assumption of a reduced steric hindrance of the *Z*-imine allowing for a closer approach to the catalyst.[3,5] However, from chemical shifts alone it is difficult to distinguish between hydrogen-bond-assisted ion pair and pure ion pair. Therefore, next the scalar couplings within and through the hydrogen bonds were investigated.

The observed $^{1}J_{HN}$ coupling constants are a measure for the binding strengths between proton and nitrogen of the imine, i.e., the larger the $^{1}J_{HN}$ the higher the ion-pair character of the binary complex. The $^{1}J_{HN}$ coupling constants of the DSI/**2a** complexes are larger than for all CPA complexes ($^{1}J_{HN}$ between 82 and 86 Hz) but still slightly smaller than the $^{1}J_{HN}$ coupling constants of the completely protonated imine with HBF_4 (Figure 4). Due to signal broadening caused by exchange processes, for the *E*-imine **2a** only the $^{1}J_{HN}$ of the complex with $(CF_3)_2$-DSI **1e** was experimentally available ($^{1}J_{HN}$ = 90.6 Hz). This coupling constant differs about 2 Hz from that observed for the completely protonated HFB_4/*E*-**2a** complex ($^{1}J_{HN}$ = 92.5 Hz) and thus reveals a very weak hydrogen bond for the $(CF_3)_2$-DSI **1e**/**2a** complex. In addition, the $^{1}J_{HN}$ coupling constants for the DSI/*Z*-imine complexes are slightly smaller than for the *E*-complexes. This confirms the stronger hydrogen bonds of the *Z*-imines, which were already discussed within the chemical shift analysis section. In accordance with this trend and the high acidity of DSI, the coupling constants for both *Z*-**2a** complexes with DSIs **1e** and **1f** ($^{1}J_{HN}$ = 88.8 Hz for both) are larger than those of the CPA complexes ($^{1}J_{HN}$ between 80 and 85 Hz) and smaller than the respective *E*-complexes as well as the protonated imine with HBF_4 ($^{1}J_{HN}$ = 92.6 Hz). These observations show unambiguously that for the *Z*-complexes a hydrogen-bond-assisted ion pair is present.

Next, potential trans-hydrogen bond scalar couplings ($^{1h}J_{NH}$ and $^{2h}J_{NN}$) were addressed since for magnetization transfers via

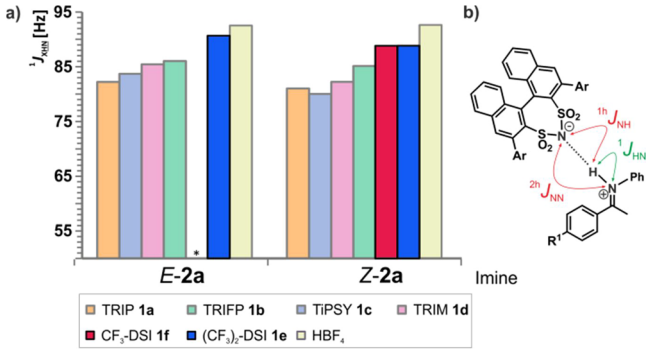

Figure 4. (a) Experimental $^{1}J_{HN}$ coupling constants are shown for *E*- and *Z*-imine **2a** with the CPAs **1a**−**1d**,[3,5] HBF_4,[3] and the DSIs **1e** and **1f** (for values, see the SI). Due to fast chemical exchange, the $^{1}J_{HN}$ of **1f**/*Z*-**2a** could not be determined (marked by an asterisk). (b) The (green) $^{1}J_{HN}$ and trans-hydrogen bond scalar couplings (red $^{1h}J_{NH}$ and $^{2h}J_{NN}$) were addressed.

$^{2h}J_{NN}$ scalar couplings across NHN hydrogen bonds large coupling constants are expected. The first trans-hydrogen bond scalar coupling was measured across such hydrogen bonds between the nitrogen atoms of Watson−Crick base pairs in ^{15}N-labeled RNA and were unexpectedly large through hydrogen bond scalar couplings of $^{2h}J_{NN} \approx 7$ Hz.[35] We also noted that $^{3h}J_{NC}$ scalar couplings through COHN hydrogen bonds could be detected in proteins. Due to the additional bond, the observed scalar coupling constants were 1 order of magnitude smaller (i.e., $^{3h}J_{CN}$ = 0.2−0.9 Hz)[36] than the $^{2h}J_{NN}$ coupling constants. Surprisingly, in our previous study of the CPA/imine complexes for the POHN hydrogen bonds (similar to the protein situation), very large trans-hydrogen bond scalar couplings of $^{3h}J_{PN} \approx 2-3$ Hz were measured, indicating the formation of strong, charge-assisted hydrogen bonds.[3] Comparable to the situation in RNA, also in the DSI complexes the additional oxygen atom within the hydrogen bond is missing. Therefore, compared to the $^{3h}J_{PN}$ coupling constants of the CPA complexes, by far stronger trans-hydrogen bond $^{2h}J_{NN}$ scalar couplings were expected for hydrogen bonds with similar strengths. For more ionic DSI complexes, these through hydrogen bond scalar couplings should be the best sensor to probe the existence of weak hydrogen bonds. However, even with ^{15}N-labeled DSI **1e** neither the $^{2h}J_{NN}$ coupling nor the $^{1h}J_{NH}$ coupling between the acidic proton and DSI nitrogen (see Figure 4b) were detectable in a 1D ^{15}N or 2D $^{1}H,^{15}N$-HSQC spectrum. Therefore, theoretical calculations were conducted and revealed for the **1e**/*E*-**2a** complex a very small $^{1h}J_{NH}$ coupling constant of 0.5 Hz and a $^{2h}J_{NN}$ coupling constant of 7 Hz. These values are in accordance with the previously found through hydrogen bond scalar couplings of Watson−Crick base pairs in ^{15}N-labeled RNA.[35] However, considering the line widths of the hydrogen bonded proton of the *Z*-complex in the ^{1}H spectrum (half line widths ~22.9 Hz), it is typical for conformational exchange and in none of the $^{1}H,^{15}N$-spectra are through hydrogen bond cross peaks detectable. Additionally, the ^{15}N signal of the free labeled DSI is sharp (half line widths ~3.5 Hz), while the ^{15}N signal of the DSI in the binary complex is broadened significantly (for spectra, see the SI). Again, this line broadening suggests exchange processes, which would also explain the missing cross peaks via partial decoupling.

DOI: 10.1021/acs.joc.9b01811
J. Org. Chem. 2019, 84, 13221−13231

Overall, the hydrogen bond analysis based on ^{1}H and ^{15}N chemical shift as well as $^{1}J_{HN}$ coupling constant revealed in all investigated DSI complexes the formation of weak charge-assisted hydrogen bonds. Due to the higher acidity of the catalyst, the hydrogen bonds and the related effect as structural anchor are weakened compared to the CPAs. However, even with ^{15}N-labeled DSI it was not possible to detect any through hydrogen bond coupling (neither the $^{2h}J_{NN}$ coupling nor the $^{1h}J_{NH}$ coupling). This observation in combination with the line broadening of the ^{15}N-signal of the DSI in the binary complex suggests several exchange processes.

Structural Investigations of the *N*-Aryl Imine Complexes. To address the potential exchange processes suggested by the hydrogen bond analysis, next the structural investigations of the DSI/imine complexes were conducted. In this way, the structural changes caused by the transition from strong to weak hydrogen bonds in the binary Brønsted acid/imine complexes should be revealed. Furthermore, in this manner, the differences of a single versus a multiple hydrogen bond acceptor catalyst within this system should become obvious.

In our previous studies of the CPA complexes for each imine isomer, two different orientations of the imine (type IE, type IIE, type IZ, and type IIZ) in the binary complex were found.[4,20] These core structures are independent of the CPA and the substitution of the *N*-arylimine. In principle, two different exchange pathways between types I and II are possible: Either the imine tilts inside the binary complex and switches the oxygen that constitutes the hydrogen bond or the imine rotates around 180° under retention of the hydrogen bond. Although types I and II are in fast exchange on the NMR time scale even at 180 K, it was possible to identify the effective exchange modes between the two orientations experimentally.[4,20] For the *E*-imine in most of the investigated complexes exclusively the tilting pathway was observed (with exception of TRIM), whereas for the *Z*-imines a combination of tilting and rotation was found.[4,20] These tilting and rotation processes are fast on the NMR time scale. In contrast, the exchange of the free imine with the imine in the binary CPA complex (dissociation/association of the imine) is slow on the NMR time scale.[4,20]

Due to the significantly weaker hydrogen bonds in the DSI/imine complexes and the five readily accessible hydrogen-binding sites of the DSI (Figure 5), additional exchange processes compared to CPAs were expected. Thus, for the first time, a fast exchange between the free imine and the *E*-imine in the binary complex was observed in the ^{1}H spectrum at 180 K (for spectra, see the SI), indicating a fast dissociation/association process of the *E*-imine. In addition, different sets of signals are observed for the *E*- and *Z*-imines within the complexes but only one set of chemical shifts for the DSI catalyst. This hints at a slow *E*/*Z* isomerization in combination with various complex structures leading to an assimilation of the catalyst chemical shifts. Therefore, theoretical calculations were used to explore the structural space of the DSI/imine complexes. These calculations predict for the *E*-imine one most stable complex structure in which a hydrogen bond between the imine and the nitrogen of the DSI (type E_N) is formed (Figure 6a). The orientation of the imine in type E_N is equivalent to the type I *E* structure of the CPA complexes. In addition, various structures with a hydrogen bond to one of the oxygens (type E_O) were found, whereby two of these orientations are energetically preferred. One of them corresponds to type I *E* (here type I E_O) and the other to type II *E* (here type II E_O) of the CPA complexes (Figure 6b). In general, the calculations predict a stronger hydrogen bond to the nitrogen than to the different oxygens. Furthermore, initial molecular dynamic calculations predict that for the exchanges between the different orientations of the imine not

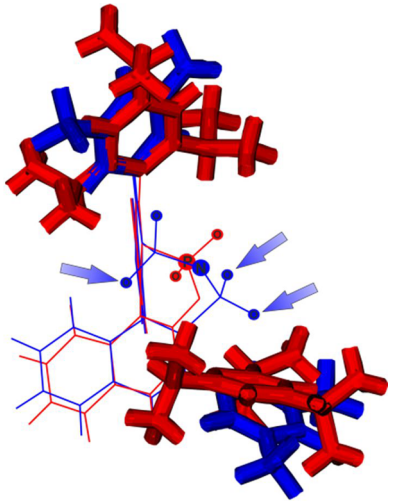

Figure 5. Overlay of TRIP **1a** (red) and $(CF_3)_2$-DSI **1e** (blue) showing the differences of the binding pockets (oxygen, phosphorus and nitrogen atoms are marked in respective colors). Indeed, the binding pocket of DSI is just slightly larger, but the hydrogen-binding sites of the DSI (denoted with blue arrows) stick out of the binding pocket and are easily available for the substrate compared to TRIP. This in combination with the increased number of hydrogen bond acceptors may result in a higher mobility of the substrate.

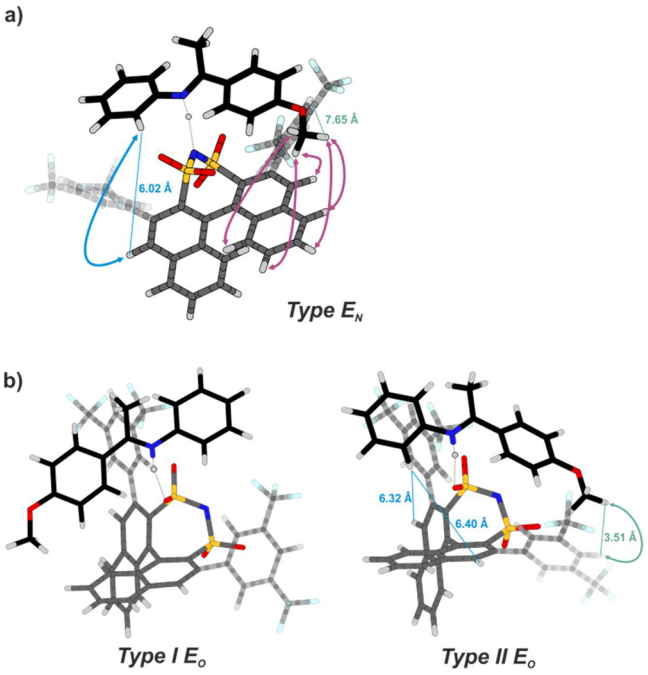

Figure 6. Calculations predict for the DSI/imine **2a** complexes the existence of (a) one stable structure where a hydrogen bond to the nitrogen of the DSI catalyst (type E_N), is formed and (b) several orientations with a hydrogen bond to one of the oxygens. The two most stable structures are shown. Type II E_o could be identified by the green NOE. All distances given in this figure were obtained from calculations.

DOI: 10.1021/acs.joc.9b01811
J. Org. Chem. 2019, 84, 13221−13231

only the tilting pathway (such as for most of the CPA complexes) but also that the rotation mechanism is active.

To confirm the predicted structures experimentally, selective 1D ^{1}H,^{1}H-NOESY as well as 2D NOESY spectra were recorded. The intense intermolecular NOEs between the *p*-methoxy group of the imine **2a** and the BINOL backbone of the DSI corroborate the existence of the energetically most favored structure (type E_N). Furthermore, the existence of the type II E_O orientation was confirmed by an NOE between the *p*-methoxy group of the imine **2a** and the 3,3′-substitents of the DSI (green arrow in Figure 6b; for spectra, see the SI). Overall, the line broadening of the ^{15}N signal of the labeled $(CF_3)_2$-DSI **1e** in the binary complex with imine **2a** (see the discussion about hydrogen bonds above), the detection of a single set of chemical shifts for the catalyst, and the observed NOEs showed experimentally that the hydrogen bond is not only formed to the strongest (here nitrogen) but also to the weaker hydrogen bond acceptors (here oxygen). Similar experimental data were found for the binary **1f**/**2a** as well as the **1f**/**2b** complex (for spectra and assignment, see the SI).

Next, the structures of the DSI/Z-complexes were addressed. The theoretical calculations predict no structural preference for the *Z*-complexes despite the stronger hydrogen bonds compared to the *E*-complexes (see hydrogen bond analysis above). Thus, the sterically less demanding *Z*-imine seems to enable even more structural orientations within the binary complex than the corresponding *E*-complexes. This was confirmed by various selective NOESY experiments, in which the NOE is transferred from the α-methyl-group to the whole catalyst backbone as well as to the protons on the 3,3′-substituents (for spectra, see the SI). Even at smaller mixing times (τ_{mix} = 25 ms), the same NOE pattern was observed, indicating a fast exchange between several hydrogen bonded species, which could not be identified unambiguously.

Overall, the structural investigations of three different binary DSI complexes showed a high mobility of the substrate inside the binding pocket of the DSI catalyst due to the presence of five hydrogen bond acceptors. Despite theoretical calculations propose significantly weaker hydrogen bonds to the oxygens, these hydrogen bonds and the corresponding structures are considerably populated even at 180 K. Thus, the weaker and more diverse hydrogen within DSI/imine complexes do not longer act as tight structural anchor. Finally, in the *E*-complex the energetically most stable structure (type E_N) as well as another, where the hydrogen bond is formed to one of the oxygens (type II E_O), was identified experimentally. On the other hand, for the complexes with the sterically less demanding *Z*-imines no structural preference was found. Despite this enormous flexibility of the binary complexes, the (*R*)-product is achieved in excess (imine **2a**: 70−78% ee with DSIs **1e** and **1f**, imine **2d**: 32−40% ee with DSIs **1e** and **1f**; see the SI). In DSI complexes, the conformational and structural dynamics may also stabilize noncovalent interactions or minimize steric repulsion to achieve high selectivities, as proposed previously.[37]

Reactivity Analysis of CPAs, DSIs, and BINSA in Transfer Hydrogenations. Recently, for the CPA-catalyzed transfer hydrogenation of *N*-arylimines an inverse correlation between reactivity and internal acidity was obtained.[5] This means that TRIP with the strongest hydrogen bond (i.e., the least acidic catalyst) shows the fastest overall reaction rate. Hence, we investigated whether this correlation is also applicable for catalysts with different acidic functionalities and acidities, specifically on combinations of BINSA **1g**, $(CF_3)_2$-DSI **1e**, (CF_3)-DSI **1f**, and TRIP **1a** with imine **2a** (calculated pK_a values in DMSO: BINSA **1g** −9, $(CF_3)_2$-DSI **1e** 0.05, TRIP **1a** 3−4).[38] The most acidic BINSA revealed the lowest reactivity, while the reactivity of the least acidic TRIP was found to be between the two DSIs (imine **2a**: $(CF_3)_2$-DSI **1e** > TRIP **1a** > (CF_3)-DSI **1f** > BINSA **1g**; for data, see the SI). This shows that in the case of significantly different hydrogen bond motifs the reactivity is not following the acidity of the catalysts. The same catalyst acidity−reactivity trend was also found with the structural similar imine **2d** in combination with the two DSIs and TRIP. Next, the effect of a bulkier imine **2c** was investigated in combination with $(CF_3)_2$-DSI **1e**, (CF_3)-DSI **1f**, and TRIP **1a**. However, with the bulkier imine **2c** the relative reactivity is different (imine **2c**: (CF_3)-DSI **1e** > $(CF_3)_2$-DSI **1f** > TRIP **1a**). This indicates that the reactivity is determined by both the structure of the catalyst (size of the binding pocket and acidic motif) and the properties of the substrate.

Analysis of the Binary *N*-Alkyl Imine Complexes. Interestingly, the reaction outcome of the transfer hydrogenation of the more basic *N*-alkylimines is extremely dependent on the used catalyst. While the highly acidic DSI catalysts were applied successfully and give the product in excellent yields and stereoselectivities, the less acidic CPA catalysts provided only disappointing enantioselectivities and low conversions.[9] To figure out if exclusively the high differences in acidity of the catalysts are responsible for these observations, also the precatalytic, binary complexes of imine **3a** with TRIP **1a** and $(CF_3)_2$-DSI **1e** at 180 K were analyzed.

Initially, the analysis of the binary TRIP/**3a**-complex revealed that apart from the *E*- and *Z*-complexes, various other hydrogen bonded species are present (Figure 7, top spectrum). The additional species were not identified, but selective 1D ^{1}H,^{1}H-NOESY experiments showed that in two of these species the *Z*-imine and in the third the *E*-imine is involved (for spectra, see the SI). Most probably, some of these complexes are dimeric species, which were observed

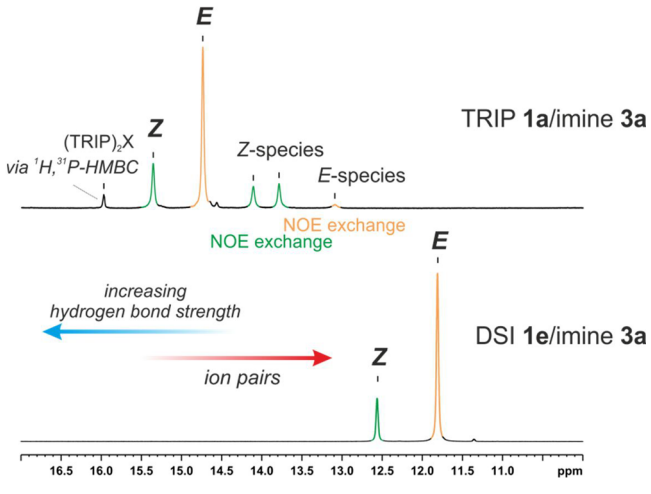

Figure 7. ^{1}H NMR spectra of the hydrogen bond region of the TRIP **1a**/**3a** and DSI **1e**/**3a** binary complexes in CD_2Cl_2 at 180 K, showing the presence of various hydrogen bonded species with TRIP. In contrast with the $(CF_3)_2$-DSI, only the major *E* and *Z* complexes were observed. On the left side of the Steiner−Limbach curve higher ^{1}H chemical shifts reveal increasing hydrogen bond strength, while smaller ^{1}H chemical shifts indicate an enhanced ion-pair character.

DOI: 10.1021/acs.joc.9b01811
J. Org. Chem. 2019, 84, 13221−13231

previously in the TRIM/*N*-arylimine complexes.[20] The population of the additional *Z*-species is significantly higher compared to the complemented *E*-species, most likely due to the less sterical demand of the *Z*-imine. Furthermore, a dimeric species of the phosphoric acid was identified.[3] Under the assumption that the transfer hydrogenation of the *N*-alkylimines also proceeds through the transition states of the *Z*-imine, as previously proposed for the *N*-arylimines,[39] these off-cycle equilibria of the *Z*-imine reduce the amount of the reactive species and may result in a reduced reactivity. Furthermore, this is the first time that we observed an enlarged structural space (two additional *Z*-imine and one additional *E*-imine complex) in the core structures of TRIP/imine complexes in comparison to our previously reported *N*-arylimine complexes,[3−5,20] which may explain the low enantioselectivity with TRIP (26% ee).

Furthermore, for the CPA catalysts a correlation between their reactivity in the transfer hydrogenation of *N*-aryl-imines and the internal acidity was found: The least acidic TRIP (i.e., forming the strongest hydrogen bond) shows the fastest overall reaction rate.[5] Thus, also the hydrogen bonds of the TRIP/**3a**-complex were analyzed. The position of the TRIP/**3a**-complexes on the Steiner−Limbach curve (see the SI) and the $^1J_{HN}$ coupling constant of the binary *E*-complex ($^1J_{HN} \approx 85$ Hz) revealed the formation of a charge-assisted hydrogen bond. However, the observed hydrogen bond is weakened compared to the CPA/*N*-arylimine complexes. The weakening of the hydrogen bond is also indicated by the fact that for the major *E*- and *Z*-complexes no magnetization is transferred from the hydrogen bonded proton to the phosphorus in a ^{1}H,^{31}P-HMBC spectrum. In contrast, for the CPA/*N*-arylimine complexes, which form stronger hydrogen bonds, this magnetization transfer was observed. Since, the weakening of a hydrogen bond comes along with an increased distance between the hydrogen-bonded proton and proton donor (TRIP), the through hydrogen bond magnetization transfer is complicated. Taking into account, that for weaker hydrogen bonds lower reactivities in the CPA-catalyzed transfer hydrogenation of *N*-arylimines were observed,[5] the even more weakened hydrogen bonds of the TRIP/*N*-alkylimine complex may also be a reason for the disappointing reactivity.

In contrast, in the ^{1}H-spectrum of the binary $(CF_3)_2$-DSI **1e**/**3a**-complex only two hydrogen bonded species, which could be assigned as binary *E*- and *Z*-complex, were observed (Figure 7, bottom spectrum). The analysis of the Steiner−Limbach curve showed that these *E*- and *Z*-complexes are positioned in the region of the pure ion pairs (see the SI). Nevertheless, the $^1J_{HN}$ coupling constant of the $(CF_3)_2$-DSI **1e**/*E*-**3a**-complex (around 91 Hz) is still slightly lower than the coupling constant in the pure ion-paired HBF_4/*E*-**2a**-complex (92.5 Hz, see above), indicating a very minor contribution of the hydrogen bond. Thus, also for the DSI/*N*-alkylimine complex the hydrogen bond is still present and can be decisive for the reactivity and selectivity. Again, a weak hydrogen bond, possible switching between various DSI hydrogen bond donors and a large binding pocket allow the mobility of the imine. These properties, coupled to the smaller size of the *N*-methyl substituent compared to *N*-phenyl, result in a fast exchange between all the possible complex structures and give only averaged NMR signals for each *E*- and *Z*-configurations even at 180 K. In addition, an *N*-tosylimine in a binary complex with TRIP was investigated to test the effect of multiple H-bond acceptors on the substrate side. Unexpectedly, no POHN hydrogen bond but instead several POHO bonds were found. This shows that multiple acceptors also on the substrate side create structural diversity (for details, see SI section 11).

Overall, the analysis of TRIP **1a**/*N*-methylamine complex showed the presence of various hydrogen-bonded species, which might lower the reactivity and selectivity due to the competition and off-cycle equilibria. For highly acidic DSI **1e**/*N*-methylamine complex, only two structures, specifically an *E*- and a *Z*-complex, were observed. In this case, off-cycle equilibria were not detectable. This may give a hint that the change in core structures could be decisive for the reaction outcome.

■ CONCLUSION

A hydrogen bond analysis of the binary complexes consisting of imines and disulfonimide (DSI) catalysts is performed and compared to chiral phosphoric acid (CPA) catalysts. With the highly acidic DSI catalysts, complexes with a high ion-pair character were formed, but unexpectedly still weak hydrogen bonds were detected. By means of NMR spectroscopy, these hydrogen bonds were analyzed using the Steiner−Limbach curve and the chemical shifts as well as the observed $^1J_{NH}$ coupling constants suggest the formation of very weak hydrogen bonds. Exchange line broadening and the lack of magnetization transfers across hydrogen bonds indicate several exchange processes of the imine.

The weakening of the structural anchor allows a high mobility of the substrate inside the pocket. Additionally, the presence of multiple hydrogen bonding sites (four oxygens and one nitrogen) results in increased structural flexibility and reveals additional entropic contributions in the DSI complexes. To identify the present species in the binary complex, a structural analysis was conducted. Calculations predicted out of a multitude of structures three energetically most favored *E*-imine complexes (type E_N, type I E_O, and type II E_O) in a fast exchange via rotation and dissociation. Even though these processes are fast on the NMR time scale, the existence of at least two structures with a hydrogen bond to the nitrogen or oxygen (type E_N and type II E_O) were confirmed by various NOESY measurements. Thus, the experiments show that not only the strongest possible hydrogen acceptor (nitrogen) is engaged in hydrogen bonding, which should be considered in the future development of catalyst design.

In the transfer hydrogenation of *N*-alkylimines, CPAs exhibit low activity and selectivity compared to DSIs. In comparison to the previously investigated *N*-arylimines, for an *N*-alkylimine several additional complex structures with TRIP were found. These additional structures and their equilibria may contribute to the poor performance of TRIP. In contrast, for the corresponding DSI complexes only the typical binary *E*- and *Z*-complexes were observed.

Overall, this study shows that a high structural flexibility is not in contrast to a good performance of a catalytic system.

■ EXPERIMENTAL SECTION

Deuterated solvents were purchased from Deutero or Sigma-Aldrich. Where anhydrous solvents were essential, CD_2Cl_2 was freshly distilled over CaH_2 under argon atmosphere. The catalysts were purchased from Sigma-Aldrich.

Synthesis of Imine Substrates. The imines were prepared according to a modified literature procedure.[3,39] The toluene was used either in p.A. quality or was dried by refluxing over sodium. The used

DOI: 10.1021/acs.joc.9b01811
J. Org. Chem. 2019, 84, 13221−13231

^{15}N-enriched aniline was purchased from Sigma-Aldrich. All imines were synthesized in accordance to our previous publications.[3,39]

*(E)-1-(4-Methoxyphenyl)-N-phenylethan-1-imine (98% ^{15}N) (**2a**).* Molecular sieves 4 Å (9.8 g) were activated at 450 °C under reduced pressure. Under argon atmosphere 4-methoxyacetophenone (2.16 g, 14.3 mmol, 1.3 equiv) and aniline (98% ^{15}N, 1 mL, 1.02 g, 11.0 mmol) were added to the Schlenk flask and dissolved in 33 mL of toluene. The solution was heated to reflux in an oil bath overnight with a drying tube filled with $CaCl_2$. The molecular sieves were removed, and the orange solution was concentrated under reduced pressure. The remaining solid was recrystallized from diethyl ether at −20 °C. The product was obtained as yellow solid. ^{1}H NMR (400.1 MHz, CD_2Cl_2): δ_H [ppm] = 7.95 (m, 2H, aryl-H), 7.35 (m, 2H, aryl-H), 7.07 (m, 1H, aryl-H), 6.96 (m, 2H, aryl-H), 6.77 (m, 2H, aryl-H), 3.86 (s, 3H, $-OCH_3$), 2.18 (d, $^3J_{HN}$ = 1.76 Hz, $-CH_3$). ^{13}C NMR {^{1}H} (100.6 MHz, CD_2Cl_2): δ_C [ppm] = 164.5, 161.9, 152.5, 132.5, 129.3, 129.2, 123.2, 119.9, 113.9, 55.8, 17.2. ^{15}N NMR (40.5 MHz, CD_2Cl_2): δ_N [ppm] = 325.5. ^{1}H and ^{13}C spectra were in accordance with the literature.[40] For the reaction kinetics, the imine **2a** was used in its unlabeled form. The synthesis was done according to this procedure only by using unlabeled aniline.

*(E)-1-(4-Trifluoromethyl)-N-phenylethan-1-anisidine (**2b**).* Molecular sieves 4 Å (9.7 g) were activated by 450 °C under reduced pressure. Under argon atmosphere, 4-trifluoromethylacetophenone (2.72 g, 14.3 mmol, 1.3 equiv) and 4-anisidine (1.37 g, 11.0 mmol) were added to the Schlenk flask and dissolved in 33 mL of toluene. The solution was heated to reflux in an oil bath overnight with a drying tube filled with $CaCl_2$. The molecular sieves were removed, and the reaction solution was concentrated under reduced pressure. The remaining solid was recrystallized from a diethyl ether/pentane− mixture (1:1) at −20 °C. The product was obtained as yellow needles. ^{1}H NMR (400.1 MHz, CD_2Cl_2): δ_H [ppm] = 8.10 (d, $^3J_{HH}$ = 8.1 Hz, 2H), 7.71 (d, $^3J_{HH}$ = 8.3 Hz, 2H), 6.93 (m, 2H), 6.76 (dm, 2H), 3.81 (s, 3H), 2.27 (s, 3H). ^{13}C NMR {^{1}H} (100.6 MHz, CD_2Cl_2): δ_C [ppm] = 164.5, 156.7, 144.6, 143.5, 127.9, 125.6, 121.0, 114.6, 55.8, 17.4. ^{19}F NMR {^{1}H} (376 MHz, CD_2Cl_2): δ_F [ppm] = −62.9. ^{15}N NMR (40.5 MHz, CD_2Cl_2): δ_N [ppm] = 337.3.

*N,1,1-Triphenylmethanimine (**2c**).* Molecular sieves 4 Å (10.0 g) were activated by 450 °C under reduced pressure. Under argon atmosphere benzophenone (2.5 g, 14.0 mmol, 1.3 equiv) and aniline (1 mL, 1.02 g, 11.0 mmol) were added to the Schlenk flask and dissolved in 33 mL toluene. The solution was heated to reflux in an oil bath overnight with a drying tube filled with $CaCl_2$. The molecular sieves were removed, and the reaction solution was concentrated under reduced pressure. The remaining solid was recrystallized from diethyl ether at −20 °C. The product was obtained as a yellow solid. ^{1}H NMR (400.1 MHz, CD_2Cl_2): δ_H = 7.77 (m, 2H, aryl-H), 7.50 (m, 1H, aryl-H), 7.42 (m, 2H, aryl-H), 7.33−7.26 (m, 3H, aryl-H), 7.18−7.10 (m, 4H, aryl-H), 6.95 (m, 1H, aryl-H), 6.78 (m, 2H, aryl-H). ^{13}C NMR {^{1}H} (100.6 MHz, CD_2Cl_2): δ_C [ppm] = 168.3, 151.9, 139.9, 136.7, 131.1, 129.7, 129.6, 128.8, 128.8, 128.5, 128.2, 122.2, 121.0. ^{15}N NMR (60.8 MHz, CD_2Cl_2): δ_N [ppm] = 330.2.

*(E)-1-(4-Methylphenyl)-N-phenylethan-1-imine (98% ^{15}N) (**2d**).* Molecular sieves 4 Å (9.8 g) were activated by 450 °C under reduced pressure. Under argon atmosphere, 4-methylacetophenone (2.27 mL, 2.28 g, 17.0 mmol, 1.6 equiv) and aniline (98% ^{15}N, 1 mL, 1.02 g, 11.0 mmol) were added to the Schlenk flask and dissolved in 33 mL of toluene. The solution was heated to reflux in an oil bath overnight with a drying tube filled with $CaCl_2$. The molecular sieves were removed, and the reaction solution was concentrated under reduced pressure. The remaining solid was recrystallized from petroleum ether at −20 °C. The product was obtained as yellow needles. ^{1}H NMR (400.1 MHz, CD_2Cl_2): δ_H [ppm] = 7.86 (m, 2H, aryl-H), 7.34 (m, 2H, aryl-H), 7.25 (m, 2H, aryl-H), 7.06 (m, 1H, aryl), 6.76 (m, 2H), 2.40 (s, 3H, $-CH_3$) 2.18 (d, $^3J_{HN}$ = 1.76 Hz, 3H, $-CH_3$). ^{13}C NMR {^{1}H} (100.6 MHz, CD_2Cl_2): δ_C [ppm] = 165.3, 152.4, 141.2, 133.9, 129.5, 129.3, 127.5, 123.3, 119.7, 21.5, 17.4. ^{15}N NMR (40.5 MHz, CD_2Cl_2): δ_N [ppm] = 328.9 ^{1}H and ^{13}C spectra were in accordance with the literature.[41]

*(E)-1-(4-Trifluoromethylphenyl)-N-phenylethan-1-imine (98% ^{15}N) (**2e**).* Molecular sieves 4 Å (5 g) were activated by 350 °C under reduced pressure. Under argon atmosphere, 4-trifluoromethylacetophenone (3.66 g, 19.5 mmol, 1.3 equiv) and aniline (98% ^{15}N, 1.40 mL, 1.40 g, 15.0 mmol) were added to the Schlenk flask and dissolved in 25 mL of toluene. The solution was heated to reflux in an oil bath overnight with a drying tube filled with $CaCl_2$. The molecular sieves were removed, and the reaction solution was concentrated under reduced pressure. The remaining solid was recrystallized from methanol at −20 °C. The product was obtained as yellow needles. ^{1}H NMR (400.1 MHz, CD_2Cl_2): δ_H [ppm] = 8.11 (m, 2H, aryl-H), 7.72 (m, 2H, aryl-H), 7.37 (m, 2H, aryl-H), 7.11 (m, 1H, aryl), 6.79 (m, 2H), 2.25 (s, 3H, $-CH_3$). ^{13}C NMR {^{1}H} (100.6 MHz, CD_2Cl_2): δ_C [ppm] = 164.5, 151.7, 143.2, 132.1, 129.4, 128.0, 125.6, 124.6, 123.9, 119.5, 17.5. ^{15}N NMR (40.5 MHz, CD_2Cl_2): δ_N [ppm] = 338.2. ^{19}F NMR {^{1}H} (376 MHz, CD_2Cl_2): δ_F [ppm] = −63.1. ^{1}H and ^{13}C spectra were in accordance with the literature.[42]

*(E)-N-Methyl-1-phenylethan-1-imine (**3a**).* *N*-Methylamine **3a** was synthesized following the literature procedure.[9] A solution of methylamine (33% in EtOH, 5 mL, 40 mmol, 4 equiv) was added to a flask containing molecular sieves 4 Å (2.5 g). The mixture was cooled to 0 °C, and freshly distilled acetophenone (1.2 mL, 10 mmol) was added. The mixture was stirred at rt for 3 days and filtered, and the solid residue was washed with DCM. The solvents were then evaporated under reduced pressure to give the product as a clear yellow oil (0.88 g, 66% yield). ^{1}H NMR (400.1 MHz, $CDCl_3$): δ_H [ppm] 7.82−7.75 (m, 2H), 7.42−7.33 (m, 3H), 3.33 (s, 3H), 2.23 (s, 3H). ^{13}C NMR {^{1}H} (100.6 MHz, $CDCl_3$): δ_C [ppm] 167.2, 141.2, 129.4, 128.0, 126.5, 39.5, 15.1. ^{1}H and ^{13}C spectra were in accordance with the literature.[9]

Sample Preparation of Binary Complexes in CD_2Cl_2. The DSI catalyst was weighted directly into a 5 mm NMR tube and dried for 20 min at 120 °C under reduced pressure. Under argon atmosphere the imine was added. CD_2Cl_2 (0.6 mL) and 1.0 mL of tetramethylsilane atmosphere were added to the tube. If not mentioned, a 1:1 catalyst/imine ratio was used. Despite careful sample preparation, hydrolysis of the imine could not be completely prevented. Therefore, the catalyst/imine ratios are slightly different than 1:1. A concentration of 50 mmol/L was used for all samples, except the sample with the ^{15}N-labeled DSI (30 mM). Between the measurements the samples were stored at −80 °C.

Spectrometer Data. NMR experiments were performed on Bruker Avance III HD 400 MHz spectrometer, equipped with 5 mm BBO BB-1H/D probe head with Z-Gradients and a Bruker Avance III HD 600 MHz spectrometer, equipped with a 5 mm CPPBBO BB−^{1}H/^{19}F. The temperature was controlled in the VT experiments by BVT 3000 and BVTE 3900. For NMR measurements employing standard NMR solvents 5 mm NMR tubes were used. All pulse programs used are standard Bruker NMR pulse programs. NMR data were processed, evaluated, and plotted with TopSpin 3.2. Further plotting of the spectra was performed with Corel Draw X7. ^{1}H and ^{13}C chemical shifts were referenced to TMS or the respective solvent signals. The heteronuclei ^{15}N and ^{19}F and were referenced, employing $\nu(X) = \nu(TMS) \times \Xi_{reference}/100$ according to Harris et al.[43] The following frequency ratios and reference compounds were used: $\Xi(^{15}N)$ = 10.132912 (lq NH_3) and $\Xi(^{19}F)$ = 94.094011 (CCl_3F). All pulse programs used are standard Bruker NMR pulse programs.

*Synthesis of (R)-3,3′-Bis[3,5-bis(trifluoromethyl)phenyl]-1,1′-binaphthyl-2,2′-diyl-O,O′-bis(N,N-dimethylthiocarbamate) (**6**).* To a suspension of NaH (60% suspension in mineral oil, 72 mg, 1.75 mmol, 5 equiv) in anhydrous DMF (2 mL) was added solid diol (*R*)-**5** (250 mg, 0.35 mmol). After the mixture turned red, *N,N*-dimethylthiocarbamoyl chloride (189 mg, 1.53 mmol, 4.4 equiv) was added and the mixture was stirred at 85 °C in an oil bath overnight. The mixture was cooled, another portion of NaH (5 equiv) and *N,N*-dimethylthiocarbamoyl chloride (5 equiv) was then added, and the mixture was stirred at rt for 5 days. The reaction was quenched by the addition of 2% aq KOH (20 mL), and the precipitate was filtered. The solid residue was then dissolved in DCM (20 mL) and washed with satd aq NaCl (20 mL). The layers were separated, and the aqueous

DOI: 10.1021/acs.joc.9b01811
J. Org. Chem. 2019, 84, 13221−13231

layer was extracted with DCM (20 mL). The combined organic layers were dried over $MgSO_4$ and filtered, and the solvent was evaporated under reduced pressure. The residue was purified by silica gel column chromatography (eluent hexanes/EtOAc 98:2−90:10) to give *O,O′*-thiocarbamate **6** (300 mg, 97% yield) as a white solid. ^{1}H NMR (400.3 MHz, $CDCl_3$): δ_H [ppm] 8.17−7.70 (m, 10 H), 7.60−7.27 (m, 6H), 2.04−3.12 (m, 12H). ^{19}F NMR {^{1}H} (376.5 MHz, $CDCl_3$): δ_F [ppm] −63.21, −63.23, −63.3. ^{1}H and ^{19}F spectra were in accordance with the literature.[13] The compound exists as a mixture of rotamers.

Synthesis of (R)-3,3′-Bis[3,5-bis(trifluoromethyl)phenyl]-1,1′-binaphthyl-2,2′-diyl-S,S′-bis(N,N-dimethylthiocarbamate) (7). Solid **6** (300 mg, 0.34 mmol) was stirred at 250 °C for 75 min in an aluminum heating block. The flask was then cooled, and the residue was purified by silica gel column chromatography (eluent hexanes/EtOAc 95:5) to give *S,S′*-thiocarbamate **7** (237 mg, 79% yield) as a white solid. ^{1}H NMR (400.3 MHz, $CDCl_3$): δ_H [ppm] 8.08 (br s, 4H), 7.98 (br s, 2H), 7.95−7.90 (m, 2H), 7.86 (br s, 2H), 7.54−7.48 (m, 2H), 7.34−7.28 (m, 2H), 7.28−7.22 (m, 2H), 2.47 (br s, 12H). ^{19}F NMR {^{1}H} (376.5 MHz, $CDCl_3$): δ_F [ppm] −62.6. ^{13}C NMR {^{1}H} (100.6 MHz, $CDCl_3$): δ_C [ppm] 165.1, 144.5, 143.4, 141.1, 133.4, 132.9, 130.6 (m), 130.5 (q, J_{CF} = 32.8 Hz), 129.8, 127.9, 127.8, 127.6, 127.3, 127.2, 123.5 (q, J_{CF} = 272.6 Hz), 120.3 (m), 36.9−36.0 (m). ^{1}H and ^{13}C spectra were in accordance with the literature.[13]

Synthesis of the DSI-Precursor BINSA ***1g***. The disulfonic acid BINSA (**1g**) was synthesized according to the literature.[13] Hydrogen peroxide (30% aq, 1 mL) was added to HCO_2H (8 mL), and the mixture was stirred at rt for 1 h. A solution of **7** (227 mg, 0.257 mmol) in DCM (4 mL) was then added, and the mixture was stirred at rt for 2 h. The mixture was then filtered through a pad of silica gel and washed with DCM, and the solvents were evaporated under reduced pressure. The residue was purified by silica gel column chromatography (eluent DCM/MeOH 20:1−10:1) to give **1g** (probably as a sodium salt, 100 mg, 46% yield) as a white solid. The solid was dissolved in DCM (20 mL), washed with 6 M aq HCl (12 mL), and the aqueous layer was extracted with DCM (2 × 15 mL). The organic layers were combined, the solvent evaporated under reduced pressure and the remaining water was removed by azeotropic distillation with toluene (3 × 20 mL) to give **1g** (BINSA, 76 mg, 34%) as a brown solid. ^{1}H NMR (400.3 MHz, CD_3OD): δ_H [ppm] 8.23 (s, 4H), 7.94 (,d J = 8.2 Hz, 2H), 7.91 (s, 2H), 7.82 (s, 2H), 7.52(t, J = 7.6 Hz, 2H), 7.32 (t, J = 7.8 Hz, 2H), 7.09 (d, J = 8.6 Hz, 2H). ^{19}F NMR { ^{1}H} (376.5 MHz, CD_3OD): δ_F [ppm] −63.9. ^{13}C NMR {^{1}H} (100.6 MHz, CD_3OD): δ_C [ppm] 147.0, 139.6, 137.8, 136.7, 134.6, 134.2, 132.6, 132.1, 131.0 (q, J_{CF} = 33.0 Hz), 129.0, 128.8, 128.7, 128.3, 125.3 (q, J_{CF} = 271.8 Hz),121.3 (m). ^{1}H- and ^{13}C-spectra were in accordance with the literature.[13]

Synthesis of the ^{15}N-labeled DSI ***1e***. The ^{15}N-DSI **1e** was synthesized from its precursor BINSA **1g** using $^{15}NH_3$ (aq) (instead of 2 M NH_3 in MeOH) by following the literature procedure.[13] BINSA **1g** (90 mg, 0.110 mmol) was dissolved in thionyl chloride (2.5 mL), anhydrous DMF (10 μL) was added and the mixture was refluxed for 2 h. The solvent was then evaporated under reduced pressure. The remaining solid was triturated with anhydrous Et_2O (2 × 1 mL) to give (*R*)-3,3′-bis[3,5-bis(trifluoromethyl)phenyl]-1,1′-binaphthyl-2,2′-disulfonyl dichloride **8** as a white solid, which was used further without any purification.

As no product was detected during a reaction of **8** with aq $^{15}NH_3$ using THF as the solvent, biphasic conditions were applied: Crude sulfonic acid dichloride **8** was dissolved in $CHCl_3$ (35 mL), cooled to −15 °C and 7 M aq $^{15}NH_3$ (4 mL) was added over 5 h. The mixture was stirred at −15 °C for 24 h and then at rt for 2 days. Then 14 M aq $^{15}NH_3$ (2 mL) was added and the reaction stirred overnight. The reaction was quenched by the addition of 5% aq $KHSO_4$ (15 mL) and extracted with $CHCl_3$ (3 × 25 mL). The combined organic layers were dried over $MgSO_4$ and filtered, and the solvent was evaporated under reduced pressure. The residue was purified by silica gel column chromatography (eluent DCM/MeOH 40:1). The purified product was dissolved in DCM (5 mL) and washed with 6 M aq HCl (5 mL), and the aqueous layer was extracted with DCM (5 mL). The organic layers were combined and washed again with 6 M aq HCl (10 mL). The aqueous layer was extracted with DCM (10 mL). The organic layers were combined, the solvent was evaporated under reduced pressure, and the remaining water was removed by azeotropic distillation with toluene (6 × 20 mL) to give DSI-**1e** (16 mg) as a brown solid. ^{1}H NMR (600.0 MHz, CD_2Cl_2): δ_H [ppm] = 8.18−8.11 (m, 4H), 8.07 (br s, 2H), 8.04−7.97 (m, 4H), 7.83 (t, J = 7.8 Hz, 2H), 7.56 (t, J = 7.8 Hz, 2H), 7.27 (d, J = 8.7 Hz, 2H), 4.30−5.60 (br s). ^{13}C NMR {^{1}H} (100.6 MHz MHz, CD_2Cl_2): δ_C [ppm] = 141.2, 138.6, 134.3, 134.2, 133.6, 132.2, 130.9 (m), 130.5, 129.2, 129.0 (m), 128.7, 128.1, 123.3 (q, J_{CF} = 273.0 Hz), 122.4, 121.7 (m). ^{19}F NMR {^{1}H} (376 MHz, CD_2Cl_2): δ_F [ppm] = −62.9, −63.0. ^{15}N NMR {inverse-gated^{1}H} (40.5 MHz, $CDCl_3$): δ_N [ppm] = 200.6. The spectral data of the purified product **1e** match the published data.[13]

Structure Identification of All Binary Complexes. The structural investigations of the binary DSI complexes were performed analogously to our previous investigations.[4,20]

Selective ^{1}H NOESY, 2D ^{1}H,^{1}H-NOESY, and ^{1}H,^{19}F-HOESY spectra were used to identify the structures of complexes *E*-**2a-b**/**1e-f** in solution. All spectra were measured in CD_2Cl_2 at 180 K. One orientation (**TYPE** E_N) was identified by the NOE pattern between the varying *p*-methoxy groups of the imines **2a** and parts of the BINOL backbone of **1e** and **1f**. In the complexes *E*-**2a**/**1e,f**, the *p*-methoxy groups were excited in selective ^{1}H NOESY spectra. In the *E*-**2b**/**1f** complex, no characteristic NOEs were found to prove the existence of **TYPE** E_N. But its existence was assumed due to the computationally calculated preference for this structure. Nevertheless, one of the other orientations (**TYPE II** E_O) was identified by 2D ^{1}H,^{1}H-NOESY spectra with a mixing time of 300 ms in all investigated complexes. Here, the characteristic NOE between aniline moiety and the backbone was found. Nevertheless, in the *E*-**2a**/**1f** complex the NOE between aniline moiety and the backbone can be assumed. In contrast to the TRIP **1a**/**2b** complexes, it was not possible to excite selectively the methoxy group of the anisidine moiety of the imine **2b** due to overlap. But in 2D ^{1}H,^{1}H-NOESY, the characteristic NOEs between the methoxy group and the BINOL backbone were found.

Selective ^{1}H NOESY and 2D ^{1}H,^{1}H-NOESY spectra were used to identify the structures of complexes *Z*-**2a**,**b**/**1e−f** in solution. All spectra were measured in CD_2Cl_2 at 180 K. The selective excitation of the α-methyl-group of both *Z*-imines **2a**,**b** in selective ^{1}H NOESYs showed NOE transfer to the whole catalyst-backbone as well as to the protons on the 3,3′-substituents. Also with a mixing time of 25 ms this NOE pattern was observed. Therefore, it is impossible to identify **TYPE I** Z_N and **TYPE II** Z_N unambiguous. Nevertheless, for the **1d**/**2b** complex in the 2D ^{1}H,^{1}H-NOESY some characteristic NOEs indicate the existence of **TYPE I** Z_N and **TYPE II** Z_N.

Reaction Kinetics of the Transfer Hydrogenation. *Representative Procedure for the ex Situ Kinetics with Imine* ***2a***. A Schlenk tube with an additional attached septum was dried at 300 °C for 15 min under reduced pressure. The flask was allowed to cool and was flushed with argon. Imine **2a** (73.7 mg, 327 μmol, 1.0 equiv) and Hantzsch ester (116.0 mg, 457.8 μmol, 1.4 equiv) were weighed into the tube. The tube was evacuated and flushed with argon three times. A standard stock solution of 1,3,5-trimethoxybenzene (54 mM) in anhydrous toluene was prepared, and 3 mL of the standard stock solution was added to the tube under argon flow. The setup was put into a metal heating block and preheated to 35 °C. A catalyst stock solution was prepared by dissolving the catalyst (2.9 mM) in anhydrous toluene. To start the reaction, the catalyst stock solution (1.0 mL, 0.009 equiv, 0.9 mol % catalyst) was added to the reaction solution. After 1, 5, 10, 15, 20, 25, 30, 45, and 60 min, samples of the reaction mixture (~0.1 mL) were taken via a septum and quenched by adding to a solution of *n*-hexane (2.0 mL) and NEt_3 (10 μL, 7.3 μg, 0.072 mmol, 100 equiv based on the catalyst). The mixture was filtered through a PTFE syringe filter and analyzed by chiral HPLC. Previously, it was shown that the addition of NEt_3 quenches the reaction and that the standard does not interfere with the reaction. The kinetics with the imines **2c** and **2d** were performed at the same scale.

DOI: 10.1021/acs.joc.9b01811
J. Org. Chem. 2019, 84, 13221−13231

*HPLC Conditions. (E)-1-(4-Methoxyphenyl)-N-phenylethan-1-imine (**2a**).* CSP-HPLC, CHIRALPAK IC column (4.6 mm × 250 mm, particle size: 5 μm), eluent *n*-hexane/2-propanol 99:1, flow rate 0.9 mL/min, column compartment temperature 20 °C, λ = 220 nm. Retention times: toluene/NEt_3: τ_1 = 3.7 min; major (*R*)-amine: τ_2 = 10.8 min; minor (*S*)-amine: τ_3 = 11.8 min; 1,3,5-trimethoxybenzene: τ_4 = 16.0 min; imine **2a**: τ_5 = 25.7 min; HE-pyridine: τ_6 = 42.9 min.

*N,1,1-Triphenylmethanimine (**2c**).* CSP-HPLC, CHIRALPAK IC column (4.6 mm × 250 mm, particle size: 5 μm), eluent *n*-hexane/2-propanol 99:1, flow rate 0.9 mL/min, column compartment temperature 20 °C, λ = 220 nm. Retention times: toluene/NEt_3: τ_1 = 3.7 min; product **4c**: τ_2 = 5.1 min; imine **2c**: τ_3 = 8.6 min; 1,3,5-trimethoxybenzene: τ_4 = 16.0 min; HE-pyridine: τ_5 = 43.0 min. An aliquot from the quenched samples was diluted 4x with *n*-hexane before syringe filtering and HPLC analysis because of the high absorption of the product at higher conversion.

*(E)-1-(4-Methylphenyl)-N-phenylethan-1-imine (98% ^{15}N) (**2d**).* CSP-HPLC, CHIRALCEL OD-H column (4.6 mm × 250 mm, particle size: 5 μm), eluent *n*-hexane/*i*-propanol 98:2, flow rate 0.9 mL/min, column compartment temperature 20 °C, λ = 220 nm. t_R: toluene/NEt_3: τ_1 = 4.0 min; HE-pyridine: τ_2 = 6.3 min; minor (*S*)-amine **4d**: τ_3 = 9.2 min; 1,3,5-trimethoxybenzene: τ_4 = 9.4 min; major (*R*)-amine **4d**: τ_5 = 10.2 min; imine **2d**: τ_6 = 11.7 min. Because of the partially overlapping peaks of the minor enantiomer of the product and the standard, the enantiomeric ratio of the product was determined at 254 nm, where the standard absorbs minimally. The integral of the minor enantiomer at 220 nm was calculated from the er and the major enantiomer peak, and the integral of the standard was calculated by subtraction from the overlapping peak.

*(E)-1-(4-Trifluoromethylphenyl)-N-phenylethan-1-imine (98% ^{15}N) (**2e**).* CSP-HPLC, CHIRALPAK IA column (4.6 mm × 250 mm, particle size: 5 μm), eluent *n*-hexane/2-propanol 99:1, flow rate 0.9 mL/min, column compartment temperature 20 °C, λ = 220 nm. t_R: toluene/NEt_3: τ_1 = 7.7 min; imine **2e**: τ_2 = 15.2 min; minor (*S*)-amine **4e**: τ_3 = 16.8 min; major (*R*)-amine **4e**: τ_4 = 18.2 min; 1,3,5-trimethoxybenzene: τ_5 = 20.3 min; HE-pyridine: τ_6 = 21.9 min.

■ ASSOCIATED CONTENT

Supporting Information

The Supporting Information is available free of charge on the ACS Publications website at DOI: 10.1021/acs.joc.9b01811.

Experimental ^1H and ^{15}N chemical shifts as well as the $^1J_{HN}$ coupling constants, complete set of ^1H and ^{15}N spectra for the binary complexes, additional information about the Steiner−Limbach curve, assignments of all binary complexes in CD_2Cl_2, computational data, NOESY spectra used for the structure investigations, chromatograms of the ex situ reaction kinetics, and reaction profiles of the transfer hydrogenation (PDF)

■ AUTHOR INFORMATION

Corresponding Author

*E-mail: ruth.gschwind@chemie.uni-regensburg.de.

ORCID

Ruth M. Gschwind: 0000-0003-3052-0077

Author Contributions

§K.R. and M.Ž. contributed equally to this work.

Notes

The authors declare no competing financial interest.

■ ACKNOWLEDGMENTS

Financial support was provided by the European Research Council (ERC-CoG 614182 − IonPairsAtCatalysis) and the DFG (SPP 1807 dispersion).

■ REFERENCES

(1) Parmar, D.; Sugiono, E.; Raja, S.; Rueping, M. Complete Field Guide to Asymmetric BINOL-Phosphate Derived Brønsted Acid and Metal Catalysis: History and Classification by Mode of Activation; Brønsted Acidity, Hydrogen Bonding, Ion Pairing, and Metal Phosphates. *Chem. Rev.* **2014**, *114* (18), 9047−9153.

(2) Terada, M. Chiral Phosphoric Acids as Versatile Catalysts for Enantioselective Transformations. *Synthesis* **2010**, 1929−1982.

(3) Sorgenfrei, N.; Hioe, J.; Greindl, J.; Rothermel, K.; Morana, F.; Lokesh, N.; Gschwind, R. M. NMR Spectroscopic Characterization of Charge Assisted Strong Hydrogen Bonds in Brønsted Acid Catalysis. *J. Am. Chem. Soc.* **2016**, *138* (50), 16345−16354.

(4) Greindl, J.; Hioe, J.; Sorgenfrei, N.; Morana, F.; Gschwind, R. M. Brønsted Acid Catalysis-Structural Preferences and Mobility in Imine/Phosphoric Acid Complexes. *J. Am. Chem. Soc.* **2016**, *138* (49), 15965−15971.

(5) Rothermel, K.; Melikian, M.; Hioe, J.; Greindl, J.; Gramüller, J.; Zabka, M.; Sorgenfrei, N.; Hausler, T.; Morana, F.; Gschwind, R. M. Internal Acidity Scale and Reactivity Evaluation of Chiral Phosphoric Acids with Different 3,3′- Substituents in Brønsted Acid Catalysis. *Chem. Sci.* **2019**, DOI: 10.1039/C9SC02342A.

(6) Knowles, R. R.; Jacobsen, E. N. Attractive Noncovalent Interactions in Asymmetric Catalysis: Links between Enzymes and Small Molecule Catalysts. *Proc. Natl. Acad. Sci. U. S. A.* **2010**, *107* (48), 20678−20685.

(7) Maji, R.; Mallojjala, S. C.; Wheeler, S. E. Chiral Phosphoric Acid Catalysis: From Numbers to Insights. *Chem. Soc. Rev.* **2018**, *47* (4), 1142−1158.

(8) Akiyama, T.; Mori, K. Stronger Brønsted Acids: Recent Progress. *Chem. Rev.* **2015**, *115* (17), 9277−9306.

(9) Wakchaure, V. N.; Kaib, P. S. J.; Leutzsch, M.; List, B. Disulfonimide-Catalyzed Asymmetric Reduction of N-Alkyl Imines. *Angew. Chem., Int. Ed.* **2015**, *54* (40), 11852−11856.

(10) Nakashima, D.; Yamamoto, H. Design of Chiral N-Triflyl Phosphoramide as a Strong Chiral Brønsted Acid and Its Application to Asymmetric Diels-Alder Reaction. *J. Am. Chem. Soc.* **2006**, *128* (30), 9626−9627.

(11) Rueping, M.; Nachtsheim, B. J.; Ieawsuwan, W.; Atodiresei, I. Modulating the Acidity: Highly Acidic Brønsted Acids in Asymmetric Catalysis. *Angew. Chem., Int. Ed.* **2011**, *50* (30), 6706−6720.

(12) Rueping, M.; Kuenkel, A.; Atodiresei, I. Chiral Brønsted Acids in Enantioselective Carbonyl Activations–Activation Modes and Applications. *Chem. Soc. Rev.* **2011**, *40* (9), 4539−4549.

(13) García-García, P.; Lay, F.; García-García, P.; Rabalakos, C.; List, B. A Powerful Chiral Counteranion Motif for Asymmetric Catalysis. *Angew. Chem., Int. Ed.* **2009**, *48* (24), 4363−4366.

(14) Treskow, M.; Neudörfl, J.; Giernoth, R. BINBAM - A New Motif for Strong and Chiral Brønsteed Acids. *Eur. J. Org. Chem.* **2009**, 3693−3697.

(15) He, H.; Chen, L. Y.; Wong, W. Y.; Chan, W. H.; Lee, A. W. M. Practical Synthetic Approach to Chiral Sulfonimides (CSIs) - Chiral Bronsted Acids for Organocatalysis. *Eur. J. Org. Chem.* **2010**, 4181−4184.

(16) James, T.; Van Gemmeren, M.; List, B. Development and Applications of Disulfonimides in Enantioselective Organocatalysis. *Chem. Rev.* **2015**, *115* (17), 9388−9409.

(17) Čorić, I.; List, B. Asymmetric Spiroacetalization Catalysed by Confined Brønsted Acids. *Nature* **2012**, *483* (7389), 315−319.

(18) Liu, L.; Kaib, P. S. J.; Tap, A.; List, B. A General Catalytic Asymmetric Prins Cyclization. *J. Am. Chem. Soc.* **2016**, *138* (34), 10822−10825.

(19) Prévost, S.; Dupré, N.; Leutzsch, M.; Wang, Q.; Wakchaure, V.; List, B. Catalytic Asymmetric Torgov Cyclization: A Concise Total Synthesis of (+)-Estrone. *Angew. Chem., Int. Ed.* **2014**, *53* (33), 8770−8773.

(20) Melikian, M.; Gramüller, J.; Hioe, J.; Greindl, J.; Gschwind, R. M. Brønsted Acid Catalysis − the Effect of 3,3′-Substituents on the Structural Space and the Stabilization of Imine/Phosphoric Acid Complexes. *Chem. Sci.* **2019**, *10* (20), 5226−5234.

(21) Rueping, M.; Sugiono, E.; Azap, C.; Theissmann, T.; Bolte, M. Enantioselective Brønsted Acid Catalyzed Transfer Hydrogenation: Organocatalytic Reduction of Imines. *Org. Lett.* **2005**, *7* (17), 3781−3783.
(22) Kaupmees, K.; Tolstoluzhsky, N.; Raja, S.; Rueping, M.; Leito, I. On the Acidity and Reactivity of Highly Effective Chiral Brønsted Acid Catalysts: Establishment of an Acidity Scale. *Angew. Chem., Int. Ed.* **2013**, *52* (44), 11569−11572.
(23) Tang, W.; Johnston, S.; Iggo, J. A.; Berry, N. G.; Phelan, M.; Lian, L.; Bacsa, J.; Xiao, J. Cooperative Catalysis through Noncovalent Interactions. *Angew. Chem., Int. Ed.* **2013**, *52* (6), 1668−1672.
(24) Kim, H.; Gerosa, G.; Aronow, J.; Kasaplar, P.; Ouyang, J.; Lingnau, J. B.; Guerry, P.; Farès, C.; List, B. A Multi-Substrate Screening Approach for the Identification of a Broadly Applicable Diels−Alder Catalyst. *Nat. Commun.* **2019**, *10* (1), 1−6.
(25) Simón, L.; Goodman, J. M. A Model for the Enantioselectivity of Imine Reactions Catalyzed by BINOL-Phosphoric Acid Catalysts. *J. Org. Chem.* **2011**, *76* (6), 1775−1788.
(26) Reid, J. P.; Goodman, J. M. Goldilocks Catalysts: Computational Insights into the Role of the 3,3′ Substituents on the Selectivity of BINOL-Derived Phosphoric Acid Catalysts. *J. Am. Chem. Soc.* **2016**, *138* (25), 7910−7917.
(27) Orlandi, M.; Toste, F. D.; Sigman, M. S. Multidimensional Correlations in Asymmetric Catalysis through Parameterization of Uncatalyzed Transition States. *Angew. Chem., Int. Ed.* **2017**, *56* (45), 14080−14084.
(28) Orlandi, M.; Coelho, J. A. S.; Hilton, M. J.; Toste, F. D.; Sigman, M. S. Parametrization of Non-Covalent Interactions for Transition State Interrogation Applied to Asymmetric Catalysis. *J. Am. Chem. Soc.* **2017**, *139* (20), 6803−6806.
(29) Duarte, F.; Paton, R. S. Molecular Recognition in Asymmetric Counteranion Catalysis: Understanding Chiral Phosphate-Mediated Desymmetrization. *J. Am. Chem. Soc.* **2017**, *139* (26), 8886−8896.
(30) Maji, R.; Champagne, P. A.; Houk, K. N.; Wheeler, S. E. Activation Mode and Origin of Selectivity in Chiral Phosphoric Acid-Catalyzed Oxacycle Formation by Intramolecular Oxetane Desymmetrizations. *ACS Catal.* **2017**, *7* (10), 7332−7339.
(31) Wheeler, S. E.; Seguin, T. J.; Guan, Y.; Doney, A. C. Noncovalent Interactions in Organocatalysis and the Prospect of Computational Catalyst Design. *Acc. Chem. Res.* **2016**, *49* (5), 1061−1069.
(32) Seguin, T. J.; Wheeler, S. E. Competing Noncovalent Interactions Control the Stereoselectivity of Chiral Phosphoric Acid Catalyzed Ring Openings of 3-Substituted Oxetanes. *ACS Catal.* **2016**, *6* (10), 7222−7228.
(33) Benedict, H.; Shenderovich, I. G.; Malkina, O. L.; Malkin, V. G.; Denisov, G. S.; Golubev, N. S.; Limbach, H. H. Nuclear Scalar Spin-Spin Couplings and Geometries of Hydrogen Bonds. *J. Am. Chem. Soc.* **2000**, *122* (9), 1979−1988.
(34) Sharif, S.; Denisov, G. S.; Toney, M. D.; Limbach, H. NMR Studies of Coupled Low- and High-Barrier Hydrogen Bonds in Pyridoxal-5 ′ -Phosphate Model Systems in Polar Solution. *J. Am. Chem. Soc.* **2007**, *129* (11), 6313−6327.
(35) Dingley, A. J.; Grzesiek, S. Direct Observation of Hydrogen Bonds in Nucleic Acid Base Pairs by Internucleotide 2 J NN Couplings. *J. Am. Chem. Soc.* **1998**, *120* (33), 8293−8297.
(36) Cordier, F.; Grzesiek, S. Direct Observation of Hydrogen Bonds in Proteins by Interresidue (3h)J(NC') Scalar Couplings. *J. Am. Chem. Soc.* **1999**, *121* (7), 1601−1602.
(37) Crawford, J. M.; Sigman, M. S. Conformational Dynamics in Asymmetric Catalysis: Is Catalyst Flexibility a Design Element? *Synthesis* **2019**, *51* (5), 1021−1036.
(38) Yang, C.; Xue, X. S.; Li, X.; Cheng, J. P. Computational Study on the Acidic Constants of Chiral Brønsted Acids in Dimethyl Sulfoxide. *J. Org. Chem.* **2014**, *79* (10), 4340−4351.
(39) Renzi, P.; Hioe, J.; Gschwind, R. M. Decrypting Transition States by Light: Photoisomerization as a Mechanistic Tool in Brønsted Acid Catalysis. *J. Am. Chem. Soc.* **2017**, *139* (19), 6752−6760.
(40) Samec, J. S. M.; Bäckvall, J. E. Ruthenium-Catalyzed Transfer Hydrogenation of Imines by Propan-2-Ol in Benzene. *Chem. - Eur. J.* **2002**, *8* (13), 2955−2961.
(41) Schramm, Y.; Barrios-Landeros, F.; Pfaltz, A. Discovery of an Iridacycle Catalyst with Improved Reactivity and Enantioselectivity in the Hydrogenation of Dialkyl Ketimines. *Chem. Sci.* **2013**, *4*, 2760−2766.
(42) Malkov, A. V.; Mariani, A.; Macdougall, K. N.; Kočovský, P. The Role of Non-Covalent Interactions in the Enantioselective Reduction of Aromatic Ketimines with Trichlorosilane. *Org. Lett.* **2004**, *6* (13), 2253−2256.
(43) Harris, R. K.; Becker, E. D.; Cabral De Menezes, S. M.; Goodfellow, R.; Granger, P. NMR Nomenclature: Nuclear Spin Properties and Conventions for Chemical Shifts (IUPAC Recommendations 2001). *Concepts Magn. Reson.* **2002**, *14* (5), 326−346.

DOI: 10.1021/acs.joc.9b01811
J. Org. Chem. 2019, 84, 13221−13231